

Cross-Receiver Generalization for RF Fingerprint Identification via Feature Disentanglement and Adversarial Training

Yuhao Pan , Xiucheng Wang , Graduate Student Member, IEEE, Nan Cheng , Senior Member, IEEE, Wenchao Xu , Member, IEEE

Abstract—Radio frequency fingerprint identification (RFFI) is a critical technique for wireless network security, leveraging intrinsic hardware-level imperfections introduced during device manufacturing to enable precise transmitter identification. While deep neural networks have shown remarkable capability in extracting discriminative features, their real-world deployment is hindered by receiver-induced variability. In practice, RF fingerprint signals comprise transmitter-specific features as well as channel distortions and receiver-induced biases. Although channel equalization can mitigate channel noise, receiver-induced feature shifts remain largely unaddressed, causing the RFFI models to overfit to receiver-specific patterns. This limitation is particularly problematic when training and evaluation share the same receiver, as replacing the receiver in deployment can cause substantial performance degradation. To tackle this challenge, we propose an RFFI framework robust to cross-receiver variability, integrating adversarial training and style transfer to explicitly disentangle transmitter and receiver features. By enforcing domain-invariant representation learning, our method isolates genuine hardware signatures from receiver artifacts, ensuring robustness against receiver changes. Extensive experiments on multi-receiver datasets demonstrate that our approach consistently outperforms state-of-the-art baselines, achieving up to a 10% improvement in average accuracy across diverse receiver settings.

Index Terms—Radio frequency fingerprint identification, domain generalization, adversarial training, receiver-invariant representation.

I. INTRODUCTION

In recent years, with the rapid advancement of Internet of Things (IoT) technologies, the large-scale deployment of IoT devices across diverse applications has significantly facilitated modern life [1], [2]. However, this proliferation has also raised increasing concerns regarding network security. The growing number of connected devices creates new attack surfaces, posing challenges for reliably distinguishing between legitimate and malicious entities, particularly in wireless networks. Conventional authentication mechanisms, such as

Media Access Control (MAC) address verification, are inherently insecure, as MAC addresses can be easily spoofed. Meanwhile, advanced security protocols such as Transport Layer Security (TLS), which rely on digital certificates and involve intensive cryptographic computations, may exceed the processing capabilities of low-power IoT devices (e.g., smart home sensors), thereby limiting their applicability in resource-constrained settings. These challenges collectively underscore the need for lightweight, hardware-level authentication mechanisms that can operate effectively in IoT environments with limited resources.

One promising solution is Radio Frequency Fingerprint Identification (RFFI), which addresses the aforementioned limitations from a physical-layer perspective. RFFI is founded on intrinsic hardware impairments introduced during the manufacturing of wireless devices. Despite identical design specifications, mass-produced devices exhibit subtle variations in electrical properties, such as resonance frequency, impedance matching, and nonlinear behavior. These physical-layer characteristics serve as unique identifiers, enabling device-level authentication without additional cryptographic overhead. Leveraging this intrinsic property, RFFI has emerged as an effective approach for device identification and classification. In recent years, RFFI has attracted increasing research attention and has also begun to find applications in commercial domains. For instance, in the Automatic Dependent Surveillance Broadcast (ADS-B) system for air traffic control, RFFI has been applied to aircraft identification and classification. This growing interest has catalyzed the technical evolution of RFFI, leading to increasingly sophisticated methods for extracting and exploiting device-specific features.

The development of RFFI techniques can generally be categorized into two main phases: traditional signal processing approaches and deep learning-based methods. In the early phase, signal processing techniques were predominantly employed to extract RFFI features from received signals. These handcrafted features are typically derived from either the waveform domain or the modulation domain. Waveform-domain features include instantaneous amplitude, instantaneous phase, instantaneous frequency, power spectral density, and wavelet-based descriptors [3], [4]. Modulation-domain features, on the other hand, involve impairments such as in-phase/quadrature (I/Q) data offsets, frequency offsets, carrier frequency offset (CFO), and differential constellation trajec-

Yuhao Pan and Wenchao Xu are with the Division of Integrative Systems and Design, Hong Kong University of Science and Technology, Hong Kong, China (e-mail:ypanca@connect.ust.hk, wenchaoxu@ust.hk). Wenchao Xu is the corresponding author.

Xiucheng Wang and Nan Cheng are with the State Key Laboratory of ISN and School of Telecommunications Engineering, Xidian University, Xi'an 710071, China (e-mail:xcwang_1@stu.xidian.edu.cn; dr.nan.cheng@ieee.org).

tory maps [5]–[7]. Such approaches rely heavily on manual feature engineering and expert domain knowledge, which limits their applicability in end-to-end learning scenarios. In recent years, with the rapid advancement of artificial neural networks, deep learning has demonstrated remarkable success in image classification and object recognition. Consequently, many researchers have applied deep learning techniques to RFFI. Convolutional Neural Networks (CNNs), in particular, have shown strong capability in capturing both spatial and temporal local features. Several studies have explored CNN-based approaches to directly extract features from raw I/Q signals, thereby reducing reliance on manual feature engineering and achieving competitive classification accuracy. For instance, Shen et al. [8] proposed a LoRa signal fingerprinting method, where coarse and fine CFO compensation were performed before applying CNNs to extract and classify device-specific RFF features. Similarly, Gopalakrishnan et al. [9] highlighted the limitation of treating I/Q signals as two independent channels, which could lead to the loss of inter-channel correlations. To address this issue, they modified convolutional layer weights to be complex-valued and employed complex convolutional kernels for processing I/Q signals. Nevertheless, although deep learning has reduced dependence on expert-designed features, the robustness and generalization of RFFI under real-world conditions remain open challenges.

To enhance robustness under dynamic wireless conditions, recent studies have proposed various methods to mitigate channel-induced variability. In real-world communication scenarios, collected I/Q signals inherently embed channel-specific characteristics, leading models to inadvertently learn these features during training. Given the dynamic nature of wireless channels, deploying a trained model in a new environment often results in degraded classification performance. Several studies have addressed this issue from different perspectives [10]–[12]. Sankhe et al. [13] considered channel dynamics and applied signal compensation techniques, and demonstrated that the Earth Mover’s Distance (EMD) between signals from the same device remains relatively low under varying channel conditions. Shen et al. [14] investigated the effects of multipath propagation and Doppler shifts on signal acquisition, using a triplet loss function to train a feature extractor based on a CNN, followed by a K-Nearest Neighbors (KNN) classifier for the identification of rogue devices. Hanna et al. [15] enhanced temporal robustness through channel equalization to mitigate wireless channel variations. Nevertheless, these works primarily focus on the transmitter-to-channel relationship, often neglecting the influence of receiver hardware variations.

The receiver-induced bias, though often overlooked, represents a critical challenge in practical RFFI systems. Most existing methods are developed and evaluated under the assumption that the same receiver is used during both training and testing. This assumption neglects the distribution shift introduced by receiver hardware discrepancies, leading to significant performance degradation when models are deployed on unseen receivers. Such limitations pose substantial risks in real-world deployments, where system functionality may be impaired if the training receiver becomes unavailable owing to hardware failures or replacement. To address this challenge,

we propose a more realistic and demanding generalization scenario: models are trained on data collected from one group of receivers and are required to generalize directly to a different set of unseen receivers. This cross-receiver generalization setting is practically important, as it enables seamless model migration and ensures continuous operation in the event of receiver replacement or malfunction.

Building upon this setting, we design a robust learning framework named Disentangled Representation for Invariant Fingerprint Training (DRIFT). In our formulation, the training data collected from multiple receivers are treated as source domains, while the test data collected from unseen receivers constitute the target domain, assuming that both domains share the same label space. Each source domain corresponds to signals received from multiple transmitters by a single receiver. The proposed framework first performs channel equalization on multi-receiver I/Q signals to suppress channel-induced noise, and then disentangles the learned representation into transmitter-specific and receiver-specific components. Cross-entropy losses are employed to supervise the extraction of both feature types, while a distance-based regularization term is introduced to improve their separability. To achieve domain invariance, a gradient reversal layer (GRL) is applied to the transmitter-specific features for adversarial alignment across receivers. For receiver-specific features, it can be observed that signals from different transmitters but received by the same receiver are expected to share similar receiver characteristics. Hence, a style transfer mechanism is incorporated to purify and enhance the consistency of receiver-specific features. The main contributions of this paper are summarized as follows:

- 1) We provide a theoretical analysis of how received I/Q signals are affected by both transmitter and receiver hardware characteristics, and propose a feature disentanglement method to separate transmitter-specific and receiver-specific components.
- 2) We explicitly incorporate the physical characteristics of wireless communication into the design. A GRL is employed to achieve domain alignment for transmitter-specific features, while a center distance loss is introduced to purify receiver-specific features via style transfer.
- 3) We conduct extensive experiments on publicly available datasets to validate the effectiveness of the proposed method. Comparisons with existing approaches demonstrate the robustness and stability of our algorithm.

The remainder of this paper is organized as follows. Section II reviews related work. Section III formulates the problem and presents the modeling of the optimization objective. Section IV provides a theoretical analysis to validate the effectiveness of the proposed algorithm. Section V evaluates the performance of our method through experiments. Finally, Section VI concludes the paper and discusses potential directions for future research.

II. RELATED WORKS AND PRELIMINARY

Deep learning-based approaches have demonstrated strong performance in RFFI. However, in real-world scenarios, dynamic channels and receiver-specific variations often lead to

domain shifts, making it difficult to extract stable transmitter-specific features. This section reviews recent research efforts to enhance the robustness and generalization capability of RFFI models in such challenging environments.

A. Deep Learning in RFFI

Recent research on RFFI has been predominantly driven by deep learning techniques, including CNNs, Long Short-Term Memory (LSTM), attention mechanisms, and Transformers. These methods aim to automatically learn discriminative features from raw RF signals. For instance, Das et al. [16] employ LSTM networks to model the temporal correlations within I/Q signal streams for the classification and identification of low-power radio devices. Merchant et al. [17] utilize a CNN-based approach on time-domain I/Q signals to achieve high identification and verification accuracy for seven ZigBee devices. Peng et al. [5] employed differential constellation trace figures to enable fine-grained recognition of hardware-level imperfections. Furthermore, Zhang et al. [18] proposed a dual attention convolutional module that adaptively assigns weights to local and global features of RF fingerprint data by attending to different feature levels. To handle varying input lengths of signal samples, Shen et al. [19] adopt a Transformer-based architecture for flexible feature extraction. Moreover, Zeng et al. [20] extended the scope from single-modality to multi-modality inputs by fusing multiple signal representations, including I/Q samples, carrier frequency offset (CFO), fast Fourier transform (FFT) coefficients, and short-time Fourier transform (STFT) coefficients, through a shared attention mechanism and concatenating the resulting features to improve classification performance.

B. Domain Adaptation in RFFI

In machine learning, distribution shifts between training and test datasets often lead to significant performance degradation of models trained solely on source domains when evaluated on unseen target domains. To address this issue, domain adaptation (DA) and domain generalization (DG) techniques have been extensively studied to enhance model robustness across diverse domains. Building upon these advances, researchers in wireless communications have employed DA methods to alleviate the performance deterioration in RFFI tasks caused by time-varying wireless channels and receiver-dependent variations.

1) *Domain Adaptation for Channel Variability*: Pan et al. [21] adopted correlation alignment (CORAL) to compensate for residual channel effects that remain after channel equalization. Chai et al. [22] proposed a multi-task learning framework with multiple classifiers to improve model robustness under varying channel conditions. Chen et al. [23] introduced a Prototype-based Domain Discrepancy Alignment (PDDA) method to mitigate distribution shifts in RFFI. Zhao et al. [24] further advanced domain adaptation by integrating a prototype model with few-shot learning to enhance generalization to unseen domains. Moreover, Wan et al. [25] proposed a robust emitter identification framework employing adversarial training and semantic consistency to extract channel-invariant features through semi-supervised domain adaptation.

2) *Domain Adaptation for Cross-Receiver RFFI*: In addition to channel variability, cross-receiver RFFI introduces additional challenges due to receiver-specific variations that cause distributional shifts across domains. To address this, several studies have investigated cross-receiver domain adaptation techniques. Zha et al. [26] leveraged the SimSiam framework for unsupervised pretraining and incorporated local maximum mean discrepancy (LMMD) as a regularization term for feature alignment, to improve generalization across receivers. Chen et al. [27] proposed a domain adaptation-based method for cross-receiver RFFI, employing a receiver discriminator to perform supervised domain alignment based on receiver labels. These methods typically assume access to unlabeled data from the target receiver domain, which allows domain adaptation to be performed during deployment.

C. Domain Generalization in RFFI

DA leverages source domain data, source domain labels, and target domain data during training to align the distributions of source and target domains. In contrast, DG relies solely on source domain data and labels without requiring access to any target domain information during training. Consequently, DG is more practical but inherently more challenging. Wang et al. [28] proposed a single-source DG approach that employs random overlay augmentation (ROA) for domain expansion and dual alignment via contrastive learning, enabling the model to extract transmitter features invariant to channel variations. Recent studies have further explored DG across different receivers. Shen et al. [14] introduced a receiver classifier branch and employed a GRL to enforce robustness in transmitter feature extraction against data collected from different receivers. Zhao et al. [29] proposed an efficient cross-receiver identification framework by pretraining the transmitter feature extraction module and subsequently fine-tuning it with data from new receivers. Zhang et al. [30] developed a model that disentangles extracted features into transmitter-independent and receiver-independent components, trained using a combination of cross-entropy loss (CE), information entropy loss (IE), and mutual independence loss (MI).

III. SYSTEM MODEL AND PROBLEM FORMULATION

A. RF Fingerprint Modeling Across Receivers

In this subsection, we present an RF fingerprint modeling process across different receivers and analyze the factors that may influence the RFFI task, as illustrated in Fig. 1.

During transmission, the analog signal is first sampled by an analog-to-digital converter (ADC) to produce a discrete digital signal that is subsequently modulated into a digital baseband signal. This digital signal is then converted into an analog baseband signal by a digital-to-analog converter (DAC), upconverted into an RF signal via a local oscillator (LO), and finally amplified by a power amplifier (PA) before transmission. During signal propagation, channel effects can further distort the transmitted signal. On the receiver side, the incoming RF signal is first amplified by a low-noise amplifier (LNA), downconverted by an LO, and digitized again by an ADC. The resulting I/Q samples serve as the input for RFFI.

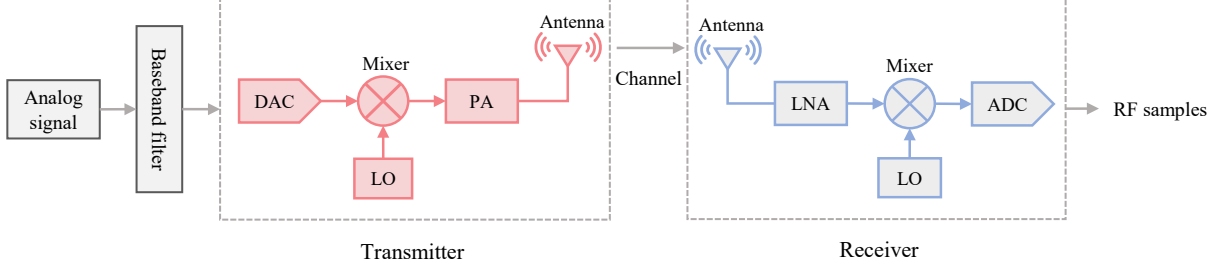


Fig. 1. Illustration of transmitter and receiver hardware impairments.

Therefore, in a cross-receiver RFFI task, the I/Q signal X_{ij}^t received by receiver j from transmitter i at time t can be modeled as:

$$X_{ij}^t = g_j \cdot h_{ij}^t \cdot f_i \cdot s_i(t) \quad (1)$$

where $s_i(t)$ denotes the baseband signal generated by transmitter i at time t , and f_i denotes hardware impairments of transmitter i , such as DAC quantization noise and PA non-linear distortion; h_{ij}^t denotes the time-varying channel response between transmitter i and receiver j , including multipath fading and noise. g_j denotes hardware impairments specific to receiver j , such as ADC quantization errors and non-linear distortion.

B. Problem Formulation

In cross-receiver RFFI, both transmitters and receivers exhibit unique hardware-specific fingerprint characteristics, as illustrated in (1). Receiver-specific features induce significant domain shifts, since the same transmitter's signal may exhibit different distributions when captured by different receivers. Specifically, for the m -th receiver, the collected dataset \mathcal{D}_s^m inherently contains receiver-specific hardware impairment features \mathbf{g}_m , which interfere with transmitter identification.

During training, we assume that I/Q signal samples are collected from M edge receiver nodes in an IoT network, with each sample originating from one of K transmitters. The entire training dataset is defined as

$$\mathcal{D}_s = \{\mathcal{D}_s^1, \mathcal{D}_s^2, \dots, \mathcal{D}_s^M\}, \quad (2)$$

where \mathcal{D}_s^m denotes the sub-dataset collected by the m -th receiver, given by

$$\mathcal{D}_s^m = \{(x_{m,i}, y_{m,i}, d_{m,i})\}_{i=1}^{N_m}, \quad (3)$$

where N_m is the total number of samples collected by receiver m , $x_{m,i}$ denotes the i -th I/Q signal sample, $y_{m,i} \in \{1, \dots, K\}$ is the corresponding transmitter label, and $d_{m,i} = m$ specifies the receiver index. Each sample is thus represented as a labeled tuple comprising the signal data, the transmitter identity label, and the receiver domain label. These receiver-specific sub-datasets are collectively utilized to train a model that generalizes to previously unseen receiver domains.

To enhance generalization in cross-receiver RFFI, our objective is to construct a robust model that is insensitive to receiver-specific features \mathbf{g}_m . This implies that features learned from data collected by M known receivers should

still enable reliable transmitter identification when deployed on an unseen $(M+1)$ -th receiver domain. Accordingly, the model should extract transmitter-specific fingerprint features while suppressing the influence of receiver-specific characteristics \mathbf{g}_m . We design a neural network classifier $f(\cdot)$ that is designed to capture intrinsic transmitter features while suppressing receiver-related factors. The training objective can be formulated as the minimization of the following loss:

$$\theta^* = \arg \min_{\theta} \mathcal{L}_{\text{CE}}(f(x; \theta), y) + \sum_j \lambda_j \mathcal{L}_{\text{reg}}^{(j)}(\theta), \quad (4)$$

where θ denotes the model parameters, \mathcal{L}_{CE} is the standard cross-entropy loss used for transmitter classification, $\mathcal{L}_{\text{reg}}^{(j)}$ represents the j -th regularization objective for enhancing cross-receiver generalization, and λ_j is a hyperparameter controlling the relative importance of the j -th regularization term.

IV. DOMAIN GENERALIZATION THEORY-BASED ANALYSIS

Traditional supervised learning methods typically rely on the assumption of independent and identically distributed (i.i.d.) samples, where both training and testing data are drawn from the same underlying distribution. However, in DG, although the source and target domains are generally assumed to share the same label space, substantial discrepancies often exist between their data distributions. The objective of DG is to train a model using data from multiple labeled source domains such that it generalizes well to unseen target domains. The central challenge lies in learning a model that achieves robust performance on distribution-shifted target domains despite having access only to source domains during training.

To systematically investigate this problem, we begin by introducing the fundamental concepts and definitions of DG. We then derive the upper bound of the generalization risk in this setting and discuss the effectiveness of the proposed framework in addressing the core challenges of DG.

A. Theoretical Analysis

1) *Notation:* Assume that the training data is drawn from multiple source domains, denoted by $\{\mathcal{D}_S^1, \mathcal{D}_S^2, \dots, \mathcal{D}_S^n\}$. Let X denote the input space and Y the label space. We assume the existence of a deterministic labeling function $f : X \rightarrow Y$, which defines the ground-truth mapping from the input space to the label space. Accordingly, each sample is represented as

a pair (x, y) , where $x \in X$ and $y = f(x) \in Y$. We define a hypothesis space \mathcal{H} , which consists of candidate prediction functions $h \in \mathcal{H}$, with each hypothesis function mapping the input space X to the label space Y , i.e., $h : X \rightarrow Y$.

The risk of a hypothesis h under distribution \mathcal{D} is defined as

$$R[h] = \mathbb{E}_{x \sim \mathcal{D}} [L(h(x), f(x))], \quad (5)$$

where $L : Y \times Y \rightarrow \mathbb{R}_+$ is a loss function measuring the discrepancy between the prediction $h(x)$ and the ground-truth label $f(x)$. This formulation quantifies the expected error of h with respect to the true labeling function f under distribution \mathcal{D} .

2) *H-Divergence*: The H-divergence is a theoretical measure used to quantify the distributional discrepancy between two domains and provides the foundation for many domain alignment methods [31]. Specifically, the H-divergence between two domains \mathcal{D}_1 and \mathcal{D}_2 under a hypothesis space \mathcal{H} is defined as

$$d_{\mathcal{H}}(\mathcal{D}_1, \mathcal{D}_2) = 2 \sup_{h \in \mathcal{H}} \left| \Pr_{x \sim \mathcal{D}_1} [h(x) = 1] - \Pr_{x \sim \mathcal{D}_2} [h(x) = 1] \right|. \quad (6)$$

where $\sup_{h \in \mathcal{H}}$ denotes the supremum over hypotheses in \mathcal{H} , and $\Pr_{x \sim \mathcal{D}_1} [h(x) = 1]$ and $\Pr_{x \sim \mathcal{D}_2} [h(x) = 1]$ denote the probabilities that hypothesis h classifies samples from \mathcal{D}_1 and \mathcal{D}_2 , respectively, as belonging to class 1. This quantity characterizes the maximum discrepancy in classification behavior that any hypothesis in \mathcal{H} can exhibit across the two domains. A larger H-divergence implies a more significant distributional discrepancy between \mathcal{D}_1 and \mathcal{D}_2 , whereas a smaller value indicates greater similarity between the two distributions.

3) *Convex Hull Definition*: For multiple source domains, we define the mixture of source distributions as the convex hull of the source domains, denoted by Λ_S . This convex hull consists of all weighted combinations of source domain distributions:

$$\Lambda_S = \left\{ \bar{D} : \bar{D}(\cdot) = \sum_{i=1}^n \pi_i D_S^i(\cdot), \pi_i \in \Delta_{N_S-1} \right\}, \quad (7)$$

where Δ_{N_S-1} represents the $N_S - 1$ -dimensional simplex, i.e., the set of all non-negative weight vectors $\pi_i \geq 0$ satisfying $\sum_{i=1}^n \pi_i = 1$.

Given an unseen target domain distribution D_U , we seek a distribution $\bar{D}_U \in \Lambda_S$ that is closest to D_U in terms of distributional divergence. Specifically, \bar{D}_U is obtained by solving the following optimization problem:

$$\bar{D}_U = \arg \min_{\pi_1, \dots, \pi_n} d_{\mathcal{H}} \left(D_U, \sum_{i=1}^n \pi_i D_S^i \right), \quad (8)$$

This formulation identifies \bar{D}_U as the optimal convex combination of source domains that most closely approximates the target domain, thus providing a theoretical foundation for enhancing model generalization to unseen domains.

Theorem 1 (Generalization Bound on Unseen Domain Risk). *Under the above setting, let S be the set of source domains, and assume the label space is $Y = [0, 1]$. For an unseen target domain distribution D_U , the risk of a hypothesis $h \in \mathcal{H}$ on*

D_U , denoted as $R_U[h]$, is upper bounded as follows [32]–[34]:

$$\begin{aligned} R_U[h] &\leq \sum_{i=1}^{N_S} \pi_i R_S^i[h] + \gamma + \epsilon \\ &\quad + \min \{E_{\bar{D}_U} [|f_{S_{\pi}} - f_U|], E_{D_U} [|f_U - f_{S_{\pi}}|]\}. \end{aligned} \quad (9)$$

Here, $R_S^i[h]$ denotes the risk of h on the i -th source domain D_S^i . The function $f_{S_{\pi}}(x) = \sum_{i=1}^{N_S} \pi_i f_{S_i}(x)$ represents the weighted combination of label functions from all source domains. The term $\gamma = d_{\mathcal{H}}(\bar{D}_U, D_U)$ is the \mathcal{H} -divergence between the target domain D_U and its closest convex combination \bar{D}_U within the convex hull of source domains. The term ϵ denotes the maximum $\tilde{\mathcal{H}}$ -divergence among all domains in the source domain set S , where $\tilde{\mathcal{H}} = \{\text{sign}(|h(x) - h'(x)| - t) \mid h, h' \in \mathcal{H}, 0 \leq t \leq 1\}$. Finally, $E_{\bar{D}_U} [|f_{S_{\pi}} - f_U|]$ and $E_{D_U} [|f_U - f_{S_{\pi}}|]$ measure the deviation between the unseen domain label function f_U and the aggregated source label function $f_{S_{\pi}}$.

B. Effectiveness of DRIFT

Based on the previous assumption that all source domains and the target domain share the same labeling function, we can further simplify Theorem 1. Specifically, assume:

$$f_{S_1} = f_{S_2} = \dots = f_{S_n} = f_U. \quad (10)$$

Under this assumption, and given that $\sum_{i=1}^n \pi_i = 1$, the aggregated label function $f_{S_{\pi}}(x)$, defined as a weighted combination of source domain label functions, simplifies to

$$f_{S_{\pi}}(x) = \sum_{i=1}^n \pi_i f_{S_i}(x) = \sum_{i=1}^n \pi_i f_U(x) = f_U(x) \sum_{i=1}^n \pi_i = f_U(x), \quad (11)$$

This implies that the aggregated label function $f_{S_{\pi}}(x)$ is identical to the target label function $f_U(x)$, i.e.,

$$|f_{S_{\pi}}(x) - f_U(x)| = 0. \quad (12)$$

Consequently, the label discrepancy term in Theorem 1 becomes zero:

$$\min \{E_{\bar{D}_U} [|f_{S_{\pi}}(x) - f_U(x)|], E_{D_U} [|f_U(x) - f_{S_{\pi}}(x)|]\} = 0. \quad (13)$$

Therefore, the risk upper bound on the unseen target domain reduces to

$$R_U[h] \leq \sum_{i=1}^{N_S} \pi_i R_S^i[h] + \gamma + \epsilon. \quad (14)$$

This simplified bound provides a theoretical foundation for RFFI domain generalization, indicating that when source and target domains share the same labeling function, the model's generalization ability on unseen domains can be improved by reducing γ and ϵ . This result motivates the use of a feature disentanglement strategy to extract transmitter-specific features while suppressing domain-specific interference introduced by receivers. Following this strategy, the disentangled feature spaces for transmitters in the source and target domains

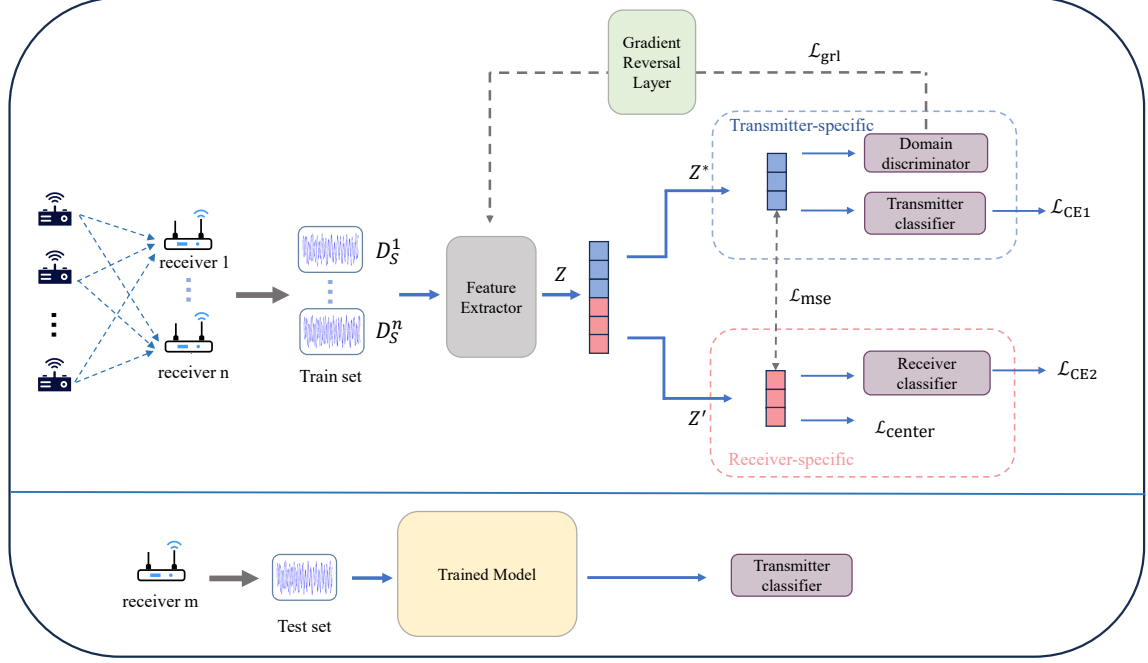


Fig. 2. Overview of the system model.

are denoted by $\{\tilde{\mathcal{D}}_S^1, \tilde{\mathcal{D}}_S^2, \dots, \tilde{\mathcal{D}}_S^n\}$ and $\tilde{\mathcal{D}}_U$, respectively. Through this separation, the source domain features exhibit increased domain invariance, thereby reducing the pairwise divergence between them, i.e., $d_H(\mathcal{D}_S^i, \tilde{\mathcal{D}}_S^j) \leq d_H(\mathcal{D}_S^i, \mathcal{D}_S^j)$, which in turn reduces ϵ . Moreover, by removing receiver-specific features within each source domain, the target domain distribution becomes easier to align with the aggregated source distribution, yielding a smaller divergence $d_H(\mathcal{D}_U, \bar{\mathcal{D}}_U) \leq d_H(\mathcal{D}_U, \tilde{\mathcal{D}}_U)$, thereby reducing γ . These reductions provide a principled explanation for the improved generalization performance achieved by our disentanglement-based approach. The detailed design of the proposed framework is presented in Section IV.

V. METHODOLOGY

Fig. 2 presents the overall architecture of DRIFT. The received signal \mathbf{x} is first passed through the feature extraction module W , yielding a representation \mathbf{z} :

$$\mathbf{z} = W(\mathbf{x}). \quad (15)$$

This representation \mathbf{z} is then disentangled into two components: the transmitter-specific feature \mathbf{z}^* and the receiver-specific feature \mathbf{z}' :

$$\mathbf{z} \mapsto \{\mathbf{z}^*, \mathbf{z}'\}. \quad (16)$$

To achieve the objective defined in (14), we employ cross-entropy loss functions to supervise the extraction of both the transmitter-specific features \mathbf{z}^* and the receiver-specific features \mathbf{z}' . Additionally, a mean squared error (MSE) loss is introduced to increase the distance between \mathbf{z}^* and \mathbf{z}' in the feature space, thereby enhancing their separability. To further align the transmitter features \mathbf{z}^* across different source domains and suppress residual receiver-specific information,

we incorporate adversarial training using a GRL during the extraction of \mathbf{z}^* . Moreover, to improve the extraction of receiver-specific features \mathbf{z}' and strengthen the disentanglement effect, we introduce an additional regularization constraint $\mathcal{L}_{\text{center}}$ (e.g., a style transfer-based constraint) on \mathbf{z}' .

A. Feature Extraction Module

In recent years, various deep neural network backbones have been applied to RFFI, including AlexNet, VGG, and ResNet [35]. Among these, ResNet effectively alleviates the degradation problem in deep neural networks through the use of residual connections, which enable the stable training of deeper models and enhance feature extraction capabilities. Accordingly, we adopt ResNet-18 as the backbone for feature extraction in our framework. Considering that the collected I/Q signals are sequential in nature and arranged as 2×256 samples, we replace the 2D convolutional layers in ResNet-18 with 1D convolutional layers to effectively capture fine-grained temporal dependencies. Specifically, the original Conv2D and BatchNorm2D layers are replaced with Conv1D and BatchNorm1D layers, respectively, to adapt the network to one-dimensional inputs. The architecture first applies a 7×1 convolution followed by a max-pooling operation to reduce the signal length and capture local temporal structures. Subsequently, four groups of residual blocks are employed to extract hierarchical representations. Finally, a global average pooling layer generates a fixed-length embedding vector $\mathbf{z} \in \mathbb{R}^{512}$, which represents the deep semantic features of the input signal.

To disentangle the transmitter-specific and receiver-specific features, we adopt a dimension-wise feature separation mechanism. The extracted 512-dimensional feature vector \mathbf{z} is partitioned into two equal sub-vectors: the first 256 dimensions represent the transmitter-specific features \mathbf{z}^* , and the remain-

ing 256 dimensions represent the receiver-specific features \mathbf{z}' . The feature extraction process is formally defined as:

$$\mathbf{z}^*, \mathbf{z}' = f_{\text{split}}(f_{\text{emd}}(\mathbf{x}; \theta)), \quad (17)$$

where \mathbf{x} denotes the input I/Q signal, θ represents the learnable parameters of the feature extractor, $f_{\text{emd}}(\cdot; \theta)$ denotes the ResNet-18-based 1D feature extraction function, and $f_{\text{split}}(\cdot)$ denotes the dimension-wise feature partitioning operation.

B. Cross-Entropy Losses

To guide the disentangled feature representations, cross-entropy losses are applied to both the transmitter classifier and the receiver classifier. Specifically, the transmitter-specific feature \mathbf{z}^* and the receiver-specific feature \mathbf{z}' , extracted from the feature encoder, are fed into the transmitter classifier $f(\cdot)$ and the receiver classifier $h(\cdot)$, respectively. Each classifier consists of three fully connected (FC) layers, followed by a softmax activation to output class probability distributions. The softmax function computes the probability that it belongs to the j -th class as:

$$\sigma_j(\mathbf{o}) = \frac{\exp(o_j)}{\sum_{k=1}^K \exp(o_k)}, \quad (18)$$

where $\mathbf{o}_y = f(\mathbf{z}^*)$ and $\mathbf{o}_d = h(\mathbf{z}')$ denote the output logits for the transmitter and receiver classifiers, respectively, and K is the number of classes. Accordingly, the predicted class labels for the transmitter and receiver are determined as:

$$\hat{y} = \arg \max_j \sigma_j(f(\mathbf{z}^*)), \quad (19)$$

$$\hat{d} = \arg \max_j \sigma_j(h(\mathbf{z}')), \quad (20)$$

where \hat{y} and \hat{d} represent the predicted transmitter and receiver labels, respectively.

The overall classification loss is defined as the sum of the transmitter classification loss \mathcal{L}_{CE1} and the receiver classification loss \mathcal{L}_{CE2} , both computed using the standard cross-entropy:

$$\mathcal{L}_{\text{CE}} = \mathcal{L}_{\text{CE1}}(f(\mathbf{z}^*), y) + \mathcal{L}_{\text{CE2}}(h(\mathbf{z}'), d), \quad (21)$$

where y and d denote the ground-truth labels for the transmitter and receiver, respectively. This objective encourages the transmitter classifier $f(\cdot)$ and the receiver classifier $h(\cdot)$ to learn discriminative features specific to the transmitter and receiver, thereby promoting feature disentanglement and improving model generalization.

C. Adversarial Training with Gradient Reversal Layer

The GRL, first introduced by Ganin et al. [36], is a widely used technique to mitigate domain shift caused by distributional discrepancies between source and target domains. It has been shown to generalize well and can be readily integrated into various neural network architectures for domain alignment. The core idea of GRL is to incorporate a domain discriminator into the network, which learns to predict the domain of origin for each input sample. During the forward pass, the GRL acts as an identity mapping and does not

alter the data flow. However, during backpropagation, it multiplies the gradient by a negative coefficient (e.g., -1 or a tunable $-\lambda$), thereby reversing the gradient direction. This adversarial mechanism forces the feature extractor to learn domain-invariant representations by confusing the domain discriminator.

In this work, although an explicit feature separation strategy is employed, the transmitter-specific features \mathbf{z}^* may still retain residual receiver-related information. To further enhance domain invariance, we incorporate GRL to align \mathbf{z}^* across receiver domains. Specifically, a GRL is inserted between \mathbf{z}^* and the transmitter classifier, and a receiver domain discriminator D is implemented as a two-layer fully connected network that outputs a probability distribution over receiver domains. The corresponding adversarial loss is defined as follows:

$$\mathcal{L}_{\text{grl}} = \mathbb{E}_{(\mathbf{z}^*, d)} [-\log D(\text{GRL}(\mathbf{z}^*))_d], \quad (22)$$

where $d \in \{1, \dots, |\mathcal{D}|\}$ denotes the receiver domain label of the input sample, and \mathcal{D} is the set of all training receiver domains. The key functionality of GRL lies in its ability to reverse the gradient during backpropagation. Formally, the GRL is defined as

$$\text{GRL}(\mathbf{z}) = \mathbf{z}, \quad (\text{forward}), \quad (23)$$

$$\frac{\partial \text{GRL}(\mathbf{z})}{\partial \mathbf{z}} = -\lambda I, \quad (\text{backward}), \quad (24)$$

where λ is a fixed or tunable coefficient. This reversed gradient enables adversarial training, suppressing residual receiver-specific information and promoting the learning of domain-invariant and transmitter-discriminative features.

D. Receiver-Specific Feature Regularization

Given the unique characteristics of I/Q signals in communication scenarios, there are notable differences compared to traditional image domain generalization. Traditional domain generalization primarily addresses variations in visual styles (e.g., sketches, cartoons, real-world images). However, in the cross-receiver RFFI task within communication systems, after applying channel equalization to mitigate the impact of channel noise, the primary differences in data distribution arise from the hardware impairments of different receivers.

In this context, I/Q signals from multiple transmitters received by the same receiver can be considered as belonging to the same domain. Since both receiver and transmitter hardware impairments affect the I/Q baseband signal in similar ways, the influence of receiver-specific features on signals from different transmitters tends to exhibit consistent patterns, resembling a style transfer effect. Consequently, the domain-specific features \mathbf{z}' extracted from the samples of different transmitters within the same domain should exhibit high similarity. Based on this observation, we introduce an auxiliary regularization task to regularize \mathbf{z}' using a center-based constraint, encouraging the domain-specific features of different transmitters under the same receiver to cluster around a common center. The corresponding center-based loss is defined as:

$$\mathcal{L}_{\text{center}} = \sum_{d \in \mathcal{D}} \frac{1}{|S_d|} \sum_{i \in S_d} \|\mathbf{z}'_i - \mathbf{c}_d\|^2 \quad (25)$$

where \mathcal{D} denotes the set of all receiver domains, S_d is the index set of samples belonging to receiver d , \mathbf{z}'_i is the domain-specific feature of the i -th sample under receiver d , and $\mathbf{c}_d = \frac{1}{|S_d|} \sum_{j \in S_d} \mathbf{z}'_j$ denotes the centroid of receiver d in the domain-specific feature space. This regularization $\mathcal{L}_{\text{center}}$ encourages samples from the same receiver domain to share similar domain-specific characteristics, promoting intra-domain compactness.

E. Feature Separation Loss

To encourage transmitter-specific and receiver-specific features to diverge in the latent space, we adopt a feature separation loss \mathcal{L}_{mse} based on MSE but defined with a negative sign. In this way, minimizing this loss term is equivalent to maximizing the distance between the two types of features, thereby enhancing disentanglement and improving the quality of feature representations. The loss is defined as:

$$\mathcal{L}_{\text{mse}} = -\frac{1}{N} \sum_{i=1}^N \|\mathbf{z}_i^* - \mathbf{z}'_i\|_2^2, \quad (26)$$

where N denotes the number of samples in a mini-batch, \mathbf{z}_i^* represents the transmitter-specific feature, and \mathbf{z}'_i represents the receiver-specific feature of the i -th sample.

F. Optimization via Backpropagation

Based on the previously introduced loss components, including the cross-entropy classification loss \mathcal{L}_{CE} , the GRL-based adversarial loss \mathcal{L}_{grl} , the receiver-specific feature regularization loss $\mathcal{L}_{\text{center}}$, and the feature separation loss \mathcal{L}_{mse} , the overall objective function of the proposed model is formulated as:

$$\mathcal{L} = \mathcal{L}_{\text{CE}} + \lambda_1 \mathcal{L}_{\text{grl}} + \lambda_2 \mathcal{L}_{\text{center}} + \lambda_3 \mathcal{L}_{\text{mse}}, \quad (27)$$

where λ_1 , λ_2 , and λ_3 are hyperparameters that control the contributions of \mathcal{L}_{grl} , $\mathcal{L}_{\text{center}}$, and \mathcal{L}_{mse} to the total loss \mathcal{L} . During training, the gradient of \mathcal{L} with respect to the feature extractor parameters θ is computed via backpropagation, and the parameters are updated via the gradient descent algorithm according to the chain rule. Algorithm 1 summarizes the training procedure of DRIFT.

VI. EXPERIMENT

A. Datasets

We utilize the open-source WiSig dataset [15], a large-scale publicly available dataset containing approximately 10 million data packets collected from 174 WiFi transmitters and 41 USRP receivers at four different time points over the course of one month. To facilitate its use in RFFI research, the dataset has been organized into four subsets: ManySig, ManyTx, ManyRx, and SingleDay. In this study, we adopt the ManySig subset, which consists of six receivers and twelve transmitters. Data were collected on four evenly spaced days within the same month, with 1000 I/Q signal samples recorded per transmitter-receiver (Tx-Rx) pair each day. All transmitters are of the model Atheros AR5212/AR5213, while the receivers belong to the USRP N210 and USRP B210 series. Transmitters

Algorithm 1 Training Procedure of DRIFT

Input: Training dataset $\mathcal{D}_s = \{\mathcal{D}_s^1, \dots, \mathcal{D}_s^M\}$
 Model parameters θ , learning rate η , total epochs T , batch size B , Hyperparameters $\lambda_1, \lambda_2, \lambda_3$
Output: Trained model parameters θ^*

```

1: for epoch = 1 to  $T$  do
2:   for each mini-batch  $\{(x_i, y_i, d_i)\}_{i=1}^B$  from  $\mathcal{D}_s$  do
3:     Extract features:  $\mathbf{z}_i = f_{\text{emd}}(x_i; \theta)$ 
4:     Split features:  $\mathbf{z}_i^*, \mathbf{z}'_i = f_{\text{split}}(\mathbf{z}_i)$ 
5:     Mean features:  $\mathbf{c}_d = \frac{1}{|S_d|} \sum_{j \in S_d} \mathbf{z}'_j$ 
6:     Classification loss  $\mathcal{L}_{\text{CE}}$ 
          $\mathcal{L}_{\text{CE1}} \leftarrow \text{CrossEntropy}(f(\mathbf{z}^*), y)$ 
          $\mathcal{L}_{\text{CE2}} \leftarrow \text{CrossEntropy}(h(\mathbf{z}'), d)$ 
          $\mathcal{L}_{\text{CE}} \leftarrow \mathcal{L}_{\text{CE1}} + \mathcal{L}_{\text{CE2}}$ 
7:     Adversarial loss  $\mathcal{L}_{\text{grl}}$ 
          $\mathcal{L}_{\text{grl}} \leftarrow \text{CrossEntropy}(D(\text{GRL}(\mathbf{z}^*)), d)$ 
8:     Center regularization loss  $\mathcal{L}_{\text{center}}$ 
          $\mathcal{L}_{\text{center}} \leftarrow \sum_{d \in \mathcal{D}} \frac{1}{|S_d|} \sum_{i \in S_d} \|\mathbf{z}'_i - \mathbf{c}_d\|_2^2$ 
9:     Feature separation loss  $\mathcal{L}_{\text{mse}}$ 
          $\mathcal{L}_{\text{mse}} \leftarrow -\frac{1}{B} \sum_{i=1}^B \|\mathbf{z}_i^* - \mathbf{z}'_i\|_2^2$ 
10:    Compute total loss:
           $\mathcal{L} \leftarrow \mathcal{L}_{\text{CE}} + \lambda_1 \mathcal{L}_{\text{grl}} + \lambda_2 \mathcal{L}_{\text{center}} + \lambda_3 \mathcal{L}_{\text{mse}}$ 
11:    Update parameters:
           $\theta \leftarrow \theta - \eta (\nabla_{\theta} \mathcal{L}_{\text{CE}} - \lambda_1 \nabla_{\theta} \mathcal{L}_{\text{grl}}$ 
           $+ \lambda_2 \nabla_{\theta} \mathcal{L}_{\text{center}} + \lambda_3 \nabla_{\theta} \mathcal{L}_{\text{mse}})$ 
12:   end for
13: end for
14: return  $\theta^*$ 

```

and receivers are labeled according to their coordinates (x, y) on the ORBIT testbed, a 20×20 grid of nodes with 3-foot (approximately 1-meter) spacing. For instance, a receiver labeled “1-1” is located at coordinate (1,1) on the ORBIT testbed. Since the objective of this study is to investigate the cross-receiver transferability of RFFI models, transmitter data observed by different receivers are regarded as distinct source domains for domain generalization.

B. Experimental Settings

To evaluate the effectiveness of the proposed algorithm, we compare it against four benchmark methods:

Algorithm 1: DANN. Proposed by Shen et al. [14], DANN introduces a transmitter classifier and a receiver classifier after the feature extraction layer. A GRL is applied before the receiver classifier to enable adversarial training, thereby improving the model’s generalization across different receiver scenarios.

Algorithm 2: RIEI. Proposed by Zhang et al. [30], RIEI disentangles the extracted features into transmitter-independent and receiver-independent representations, which are then fed into separate classifiers. MI loss and IE loss are introduced to facilitate feature disentanglement. During testing, only the transmitter classifier is utilized.

Algorithm 3: MTL. This benchmark employs a multi-task learning strategy by feeding the extracted features into both receiver and transmitter classifiers.

TABLE I
PERFORMANCE (%) OF ALL METHODS ON DIFFERENT RECEIVER COMBINATIONS

Train Receiver	Test Receiver	DANN	RIEI	MTL	ERM	DRIFT
(1-1, 14-7, 7-7)	(1-19)	53.58	54.38	54.28	<u>66.37</u>	69.93
	(19-2)	65.58	<u>67.77</u>	64.45	65.33	75.40
	(2-1)	74.03	<u>78.47</u>	63.15	63.25	90.13
	(2-19)	<u>62.78</u>	53.82	55.73	56.97	63.87
	(20-1)	48.82	50.43	<u>58.32</u>	50.42	69.70
	(7-14)	69.13	<u>69.53</u>	69.15	67.02	80.73
	(8-8)	<u>66.98</u>	62.15	65.28	61.57	79.60
	Average	<u>62.99</u>	62.36	61.51	61.56	75.62
	(1-19)	<u>62.62</u>	61.82	52.83	61.35	74.03
(1-1, 14-7, 18-2, 7-7)	(19-2)	64.23	<u>72.32</u>	61.82	56.10	74.77
	(2-1)	49.52	<u>79.68</u>	55.77	76.97	89.98
	(2-19)	<u>68.25</u>	65.22	53.65	53.43	76.35
	(20-1)	52.68	<u>68.23</u>	58.32	55.47	<u>65.75</u>
	(3-19)	56.22	49.62	<u>63.43</u>	63.33	75.42
	(7-14)	66.05	80.63	66.63	72.00	<u>79.73</u>
	(8-8)	67.22	<u>73.27</u>	69.18	71.45	80.9
	Average	60.85	<u>68.85</u>	60.20	63.76	77.12
	(19-2)	58.55	64.37	52.33	66.48	<u>64.78</u>
(1-1, 1-19, 14-7, 8-8)	(2-1)	76.25	<u>75.67</u>	71.32	67.30	74.37
	(2-19)	61.05	60.4	61.28	75.70	<u>75.4</u>
	(20-1)	46.87	39.32	<u>65.98</u>	41.32	67.32
	(7-14)	78.78	83.97	<u>84.53</u>	82.28	94.63
	(7-7)	54.63	56.08	50.00	<u>61.67</u>	68.75
	Average	62.68	63.30	64.24	<u>65.79</u>	74.21
	(19-2)	78.95	84.63	61.57	71.82	<u>80.22</u>
	(2-1)	66.67	<u>86.25</u>	77.38	69.02	92.37
	(2-19)	63.17	83.23	58.52	<u>73.38</u>	82.53
	(20-1)	58.70	67.82	62.58	51.43	<u>63.58</u>
	(7-14)	77.32	<u>84.70</u>	82.02	78.23	98.42
	Average	68.96	<u>81.33</u>	68.41	68.78	83.42

Algorithm 4: ERM. Empirical Risk Minimization (ERM) optimizes model parameters by minimizing the average loss over the training data.

In Shen et al.’s work, the feature extraction module is based on ResNet, consisting of nine convolutional layers with skip connections, each followed by a ReLU activation. Zhang et al. employ a variant of ResNet18 in which 2D convolutions are replaced with 1D convolutions to better capture the temporal characteristics of I/Q signals. To ensure a fair comparison, we adopt a unified ResNet18-1D architecture for the feature extraction module across all algorithms. Both the transmitter and receiver classifiers consist of three fully connected layers.

We train the proposed method using the Adam optimizer with a batch size of 64 and an initial learning rate of 0.0001. The hyperparameters are set as $\lambda_1 = 1$, $\lambda_2 = 0.01$, and $\lambda_3 = 0.02$, unless otherwise specified. All experiments are implemented in PyTorch 2.0.0 with Python 3.8, and conducted on a system equipped with an Intel Xeon Platinum 8255C CPU and an NVIDIA GeForce RTX 2080Ti GPU. To ensure fairness and reproducibility, we fix the random seed during training. For evaluation, we save the model checkpoints from

the last five epochs of each algorithm, and report the average performance to reduce the effect of randomness.

C. Experiment 1: Cross-Receiver Generalization

To validate the effectiveness of the proposed algorithm DRIFT, we conduct comprehensive performance comparisons on the ManySig dataset against several baseline methods, including DANN, RIEI, and MTL. To mitigate the impact of channel variation on model performance, all experiments are conducted using data from Day 1 of the dataset. During each training process, the number of I/Q samples per transmitter is set to 800. If training involves n receivers, the total number of training samples amounts to $6 \times 800 \times n$, while the testing set remains fixed at 6×200 samples. All experiments are conducted under the condition that the training and testing receivers are disjoint, in order to evaluate the cross-receiver domain generalization capability of the models.

We first evaluate the scenario where three receivers $\{1-1, 14-7, 7-7\}$ are used for training. The model is then tested on seven unseen receivers: $\{1-19, 19-2, 2-1, 2-19, 20-1, 7-14, 8-8\}$. As shown in Table I, DRIFT achieves superior performance across

TABLE II
CROSS-DAY PERFORMANCE (%) OF ALL METHODS ON DIFFERENT RECEIVER COMBINATIONS

Training Receivers	Test Receiver (Day 1 → Day n)	DANN	RIEI	MTL	ERM	DRIFT
(1-1, 1-19, 8-8)	Day 2	67.17	72.59	73.33	<u>74.35</u>	80.37
	Day 3	66.95	<u>72.96</u>	71.88	72.88	78.05
	Day 4	64.95	69.04	<u>73.45</u>	69.31	79.38
	Average	66.36	71.53	<u>72.89</u>	72.18	79.27
(1-1, 14-7, 18-2, 7-7)	Day 2	61.23	69.86	62.96	66.36	<u>69.70</u>
	Day 3	66.58	<u>70.38</u>	64.43	67.02	71.00
	Day 4	64.95	<u>67.88</u>	66.21	64.83	68.30
	Average	64.25	<u>69.37</u>	64.53	66.07	69.67
(1-1, 1-19, 14-7, 7-7, 8-8)	Day 2	<u>75.55</u>	73.90	72.43	72.97	79.12
	Day 3	<u>78.74</u>	72.47	66.15	73.30	82.10
	Day 4	69.84	68.74	<u>72.56</u>	66.80	81.64
	Average	<u>74.71</u>	71.70	70.38	71.02	80.95

all testing receivers, with an average transmitter identification accuracy of 75.62%. This significantly outperforms DANN (62.99%), RIEI (62.36%), and MTL (61.56%), demonstrating its effectiveness in cross-receiver domain generalization.

In further experiments, we increase the diversity of the training domain by incorporating additional receiver combinations. When trained with receivers {1-1, 14-7, 18-2, 7-7}, DRIFT achieves an improved average accuracy of 77.12%, surpassing DANN (62.68%), RIEI (68.85%), and ERM (63.76%). Notably, on the test receiver 2-1, DRIFT attains an accuracy of 89.98%, outperforming DANN and MTL by approximately 29% and 13%, respectively. When the training receivers are changed to {1-1, 1-19, 14-7, 8-8}, DRIFT achieves an average accuracy of 74.21%, corresponding to an 8.4% improvement over the second-best method, MTL (65.79%).

Finally, in the most challenging scenario, where the training set includes a broader range of receivers {1-1, 1-19, 14-7, 7-7, 8-8}, DRIFT achieves the highest average accuracy of 83.42%. Notably, it obtains near-perfect recognition results on test receivers 2-1 and 7-14, with accuracy rates of 92.37% and 98.42%, respectively. These results demonstrate that DRIFT consistently achieves high performance across diverse testing receivers. Overall, these experimental findings suggest that the proposed method possesses strong generalization capabilities under complex cross-receiver conditions.

D. Experiment 2: Cross-Day Model Stability

In this set of experiments, we further investigate the impact of temporal channel variations across different days on the performance of cross-receiver domain generalization models. Specifically, we use data from Day 1 for training and evaluate the models on data collected from different receivers on Day 2, Day 3, and Day 4. This setup simulates the temporal variability of wireless channels during real-world deployments. To facilitate a clearer presentation of the results, each training configuration is evaluated on multiple unseen receivers from the target days, and the average performance across all test receivers is reported. This provides a comprehensive assessment

of each model's generalization ability and stability under time-varying channel conditions.

We select three different sets of receiver combinations for training, representing increasing levels of domain diversity:

- **Group 1:** {1-1, 1-19, 8-8} – 3 receivers
- **Group 2:** {1-1, 14-7, 18-2, 7-7} – 4 receivers
- **Group 3:** {1-1, 1-19, 14-7, 7-7, 8-8} – 5 receivers

As shown in Table II, under the first training configuration (3 receivers), DRIFT achieves an average transmitter identification accuracy of 79.27% across the three test days. This improves upon the second-best model MTL (72.18%) by 7.09%, and exceeds DANN and RIEI by 12.91% and 7.74%, respectively. Notably, on Day 2, DRIFT achieves an accuracy of 80.37%, making it the only model to surpass the 80% threshold under this setting, thereby demonstrating robustness to temporal channel perturbations. In the second training configuration (4 receivers), as domain diversity increases, DRIFT maintains strong performance, achieving an average accuracy of 69.67%, slightly outperforming RIEI (69.37%), and exceeding DANN (64.25%) and MTL (66.07%). In the third configuration, where the model is trained with the most diverse receiver set (5 receivers), performance improves across all models. However, DRIFT remains the top performer, achieving an average accuracy of 80.95% over the three days. This corresponds to a nearly 10% improvement over MTL (71.02%) and a 6.24% increase over DANN (74.71%). These results demonstrate that DRIFT effectively leverages multi-receiver data to extract transmitter features invariant to both temporal and receiver-induced variations.

E. Experiment 3: Contribution of Each Module

In this section, we conduct a comprehensive ablation study to evaluate the contributions of each key module in our proposed model to cross-receiver generalization. Training is conducted using the receiver combination {1-1, 1-19, 14-7, 7-7, 8-8}, and evaluation is performed on five unseen receivers {19-2, 2-1, 2-19, 20-1, 7-14} across four different days (Day 1 to Day 4). Table III reports the average transmitter

identification accuracies over these test receivers, allowing us to quantitatively assess the contribution of each module. The *Basic Model*, which corresponds to ERM, includes only transmitter and receiver classifiers trained with a standard cross-entropy loss, without any feature separation or regularization mechanisms. In subsequent experiments, additional modules are gradually integrated, including the GRL, center regularization (Cen), and MSE-based separation.

TABLE III
ABLATION STUDY OF EACH COMPONENT IN OUR PROPOSED METHOD

Model	Day1	Day2	Day3	Day4	Avg
Basic Model	70.59	75.87	74.76	70.99	73.05
+GRL	76.68	78.03	81.05	74.23	77.50
+Cen	75.57	78.85	82.90	78.16	78.87
+MSE	77.87	75.94	81.01	79.02	78.46
+MSE+GRL	80.32	77.26	78.84	75.75	78.04
+MSE+Cen	80.03	76.23	80.01	78.05	78.58
+GRL+Cen	69.29	72.92	74.25	67.84	71.08
Full Model	83.42	79.12	82.10	81.64	81.57

As shown in Table III, incorporating any individual module consistently improves average accuracy. Specifically, adding GRL, Cen, or MSE to the Basic Model increases average accuracy to 77.50%, 78.87%, and 78.46%, respectively. Certain combinations of modules yield further gains; for instance, the +MSE+Cen variant achieves 78.58%. However, the combination of GRL and Cen without the MSE-based separation module (i.e., +GRL+Cen) leads to performance degradation, likely due to conflicting regularization effects, indicating that module coordination is crucial.

Finally, the **Full Model**, which integrates all modules, achieves the highest average accuracy of 81.57% across all days, outperforming all other variants. These results validate the complementary nature of each component and demonstrate the effectiveness of the overall model design.

F. Experiment 4: Hyperparameter Sensitivity Analysis

In this section, we investigate the impact of three key hyperparameters on the performance of the proposed method in cross-receiver transmitter identification. To ensure a fair comparison, only one hyperparameter is varied in each experiment while keeping the others fixed at their default values ($\lambda_1 = 1$, $\lambda_2 = 0.01$, and $\lambda_3 = 0.02$), thereby enabling an accurate assessment of the individual contribution of each component. Experiments are conducted using a receiver combination of {1-1, 14-7, 18-2, 7-7} to validate hyperparameter sensitivity.

We first evaluate the effect of the GRL loss weight λ_1 . As illustrated in Fig. 3(a), λ_1 is varied from 0.1 to 5. The model achieves the best performance when $\lambda_1 = 1$ (77.12%). Performance remains relatively stable from $\lambda_1 = 0.5$ (75.21%) to $\lambda_1 = 2$ (75.23%), suggesting that moderate adversarial strength helps extract domain-invariant features relevant to the transmitter while mitigating receiver-specific interference. However, further increasing λ_1 to 3 and 5 leads to a significant performance drop (68.60% and 67.15%, respectively),

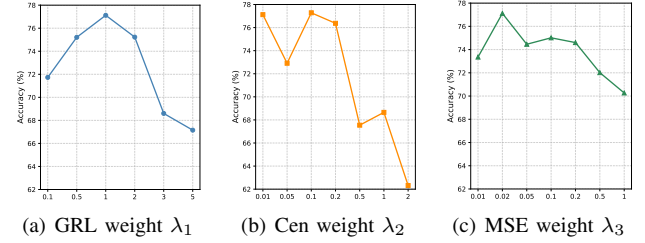


Fig. 3. Sensitivity analysis of hyperparameters λ_1 , λ_2 , and λ_3 .

indicating that excessive adversarial gradients may hinder the feature learning process and suppress discriminative transmitter information.

Next, we examine the influence of the regularization weight λ_2 for the receiver-specific feature. As shown in Fig. 3(b), the accuracy fluctuates considerably across different λ_2 values, indicating a higher sensitivity to this hyperparameter. Notably, performance drops to 72.91% when $\lambda_2 = 0.05$, but improves to 77.28% and 76.37% at $\lambda_2 = 0.1$ and $\lambda_2 = 0.2$, respectively. However, accuracy decreases again when $\lambda_2 = 0.5$ (67.54%) or larger. These results suggest that moderate regularization helps constrain the receiver-specific features to prevent overfitting to domain-specific cues, while overly strong regularization may suppress beneficial diversity, degrading model discriminability.

Finally, we analyze the sensitivity of the MSE-based feature separation loss weight λ_3 . As illustrated in Fig. 3(c), the model exhibits relatively stable performance across different λ_3 values. The best result is obtained at $\lambda_3 = 0.02$, while other settings yield comparable outcomes, indicating that λ_3 has a relatively minor impact on performance. This robustness over a wide range of values makes the choice of λ_3 less critical and enhances practical deployability.

In summary, the proposed method shows different levels of sensitivity to the three hyperparameters. The weights λ_1 and λ_2 require careful tuning to avoid training instability or over-regularization, whereas λ_3 demonstrates greater tolerance and contributes to training robustness.

VII. CONCLUSION AND FUTURE WORK

With the rapid advancement of deep learning, considerable efforts have been devoted to incorporating CNNs and other models into end-to-end RFFI frameworks to enhance feature extraction automation and identification accuracy. However, most existing methods assume a fixed receiver environment for both training and testing, overlooking the feature shifts introduced by hardware discrepancies across different receivers. To address this limitation, we propose an enhanced method under the cross-receiver scenario, with the goal of improving model robustness and adaptability to previously unseen receivers. This capability is particularly important in real-world applications where receiver failure may necessitate seamless model migration to new devices. In this work, we develop a cross-receiver generalization framework based on feature disentanglement. Specifically, the model explicitly separates transmitter-specific and receiver-specific features to achieve

effective disentanglement. A GRL is incorporated into the transmitter feature extraction pathway to encourage domain-invariant representations, while a regularization term is applied to the receiver pathway to capture domain-specific receiver characteristics. Extensive experiments conducted on an open-source dataset validate the proposed method's superior recognition accuracy and generalization ability in cross-receiver scenarios. In future work, we plan to extend the proposed framework to accommodate receivers with different signal reception formats, thereby enhancing its applicability in heterogeneous systems and advancing the practical deployment of RFFI in automated and scalable environments.

REFERENCES

- [1] W. Xu, H. Zhou, N. Cheng, F. Lyu, W. Shi, J. Chen, and X. Shen, "Internet of vehicles in big data era," *IEEE/CAA Journal of Automatica Sinica*, vol. 5, no. 1, pp. 19–35, 2017.
- [2] N. Lu, N. Cheng, N. Zhang, X. Shen, and J. W. Mark, "Connected vehicles: Solutions and challenges," *IEEE internet of things journal*, vol. 1, no. 4, pp. 289–299, 2014.
- [3] Y. Yuan, Z. Huang, H. Wu, and X. Wang, "Specific emitter identification based on hilbert-huang transform-based time–frequency–energy distribution features," *IET communications*, vol. 8, no. 13, pp. 2404–2412, 2014.
- [4] L. Ding, S. Wang, F. Wang, and W. Zhang, "Specific emitter identification via convolutional neural networks," *IEEE communications letters*, vol. 22, no. 12, pp. 2591–2594, 2018.
- [5] L. Peng, J. Zhang, M. Liu, and A. Hu, "Deep learning based rf fingerprint identification using differential constellation trace figure," *IEEE Transactions on Vehicular Technology*, vol. 69, no. 1, pp. 1091–1095, 2019.
- [6] K. Yang, J. Kang, J. Jang, and H.-N. Lee, "Multimodal sparse representation-based classification scheme for rf fingerprinting," *IEEE Communications Letters*, vol. 23, no. 5, pp. 867–870, 2019.
- [7] J. Hua, H. Sun, Z. Shen, Z. Qian, and S. Zhong, "Accurate and efficient wireless device fingerprinting using channel state information," in *IEEE INFOCOM 2018-IEEE Conference on Computer Communications*. IEEE, 2018, pp. 1700–1708.
- [8] G. Shen, J. Zhang, A. Marshall, L. Peng, and X. Wang, "Radio frequency fingerprint identification for lora using spectrogram and cnn," in *IEEE INFOCOM 2021-IEEE Conference on Computer Communications*. IEEE, 2021, pp. 1–10.
- [9] S. Gopalakrishnan, M. Cekic, and U. Madhow, "Robust wireless fingerprinting via complex-valued neural networks," in *2019 IEEE Global Communications Conference (GLOBECOM)*. IEEE, 2019, pp. 1–6.
- [10] A. Al-Shawabka, F. Restuccia, S. D’Oro, T. Jian, B. C. Rendon, N. Soltani, J. Dy, S. Ioannidis, K. Chowdhury, and T. Melodia, "Exposing the fingerprint: Dissecting the impact of the wireless channel on radio fingerprinting," in *IEEE INFOCOM 2020-IEEE Conference on Computer Communications*. IEEE, 2020, pp. 646–655.
- [11] X. Wang, K. Tao, N. Cheng, Z. Yin, Z. Li, Y. Zhang, and X. Shen, "Radiodiff: An effective generative diffusion model for sampling-free dynamic radio map construction," *IEEE Transactions on Cognitive Communications and Networking*, 2024.
- [12] X. Wang, Q. Zhang, N. Cheng, R. Sun, Z. Li, S. Cui, and X. Shen, "Radiodiff- k^2 : Helmholtz equation informed generative diffusion model for multipath-aware radio map construction," *arXiv preprint arXiv:2504.15623*, 2025.
- [13] K. Sankhe, M. Belgiovine, F. Zhou, S. Riyaz, S. Ioannidis, and K. Chowdhury, "Oracle: Optimized radio classification through convolutional neural networks," in *IEEE INFOCOM 2019-IEEE conference on computer communications*. IEEE, 2019, pp. 370–378.
- [14] G. Shen, J. Zhang, A. Marshall, and J. R. Cavallaro, "Towards scalable and channel-robust radio frequency fingerprint identification for lora," *IEEE Transactions on Information Forensics and Security*, vol. 17, pp. 774–787, 2022.
- [15] S. Hanna, S. Karunaratne, and D. Cabric, "Wisig: A large-scale wifi signal dataset for receiver and channel agnostic rf fingerprinting," *IEEE Access*, vol. 10, pp. 22 808–22 818, 2022.
- [16] R. Das, A. Gadre, S. Zhang, S. Kumar, and J. M. Moura, "A deep learning approach to iot authentication," in *2018 IEEE international conference on communications (ICC)*. IEEE, 2018, pp. 1–6.
- [17] K. Merchant, S. Revay, G. Stantchev, and B. Nousain, "Deep learning for rf device fingerprinting in cognitive communication networks," *IEEE journal of selected topics in signal processing*, vol. 12, no. 1, pp. 160–167, 2018.
- [18] W. Zhang, W. Zhao, X. Tan, L. Shao, and C. Ran, "Adaptive rf fingerprints fusion via dual attention convolutions," *IEEE Internet of Things Journal*, vol. 9, no. 24, pp. 25 181–25 195, 2022.
- [19] G. Shen, J. Zhang, A. Marshall, M. Valkama, and J. R. Cavallaro, "Toward length-versatile and noise-robust radio frequency fingerprint identification," *IEEE Transactions on Information Forensics and Security*, vol. 18, pp. 2355–2367, 2023.
- [20] Y. Zeng, Y. Gong, J. Liu, S. Lin, Z. Han, R. Cao, K. Huang, and K. B. Letaief, "Multi-channel attentive feature fusion for radio frequency fingerprinting," *IEEE Transactions on Wireless Communications*, vol. 23, no. 5, pp. 4243–4254, 2023.
- [21] R. Pan, H. Chen, H. Chen, and W.-Q. Wang, "Equalization assisted domain adaptation for radio frequency fingerprint identification," *IEEE Wireless Communications Letters*, 2024.
- [22] Z. Chai, X. Peng, X. Huang, M. Li, and X. Yang, "Channel-robust rf fingerprint identification using multi-task learning and receiver collaboration," *IEEE Signal Processing Letters*, 2024.
- [23] J. Chen, L. Yu, Y. Chen, X. Zheng, P. Chen, and K. Cheng, "Prototype-driven unsupervised domain adaptation for specific emitter identification," *IEEE Internet of Things Journal*, 2024.
- [24] T. Zhao, X. Wang, and S. Mao, "Cross-domain, scalable, and interpretable rf device fingerprinting," in *IEEE INFOCOM 2024-IEEE Conference on Computer Communications*. IEEE, 2024, pp. 2099–2108.
- [25] H. Wan, Q. Wang, X. Fu, Y. Wang, H. Zhao, Y. Lin, H. Sari, and G. Gui, "Vc-sei: Robust variable-channel specific emitter identification method using semi-supervised domain adaptation," *IEEE Transactions on Wireless Communications*, 2024.
- [26] X. Zha, T. Li, Z. Qiu, and F. Li, "Cross-receiver radio frequency fingerprint identification based on contrastive learning and subdomain adaptation," *IEEE Signal Processing Letters*, vol. 30, pp. 70–74, 2023.
- [27] Z. Chen, Z. Pang, W. Hou, H. Wen, M. Wen, R. Zhao, and T. Tang, "Cross-device radio frequency fingerprinting identification based on domain adaptation," *IEEE Transactions on Consumer Electronics*, vol. 70, no. 1, pp. 2391–2400, 2024.
- [28] Y. Wang, T. Ohtsuki, Z. Sun, D. Niyato, X. Wang, and G. Gui, "Avoiding shortcuts: Enhancing channel-robust specific emitter identification via single-source domain generalization," *IEEE Transactions on Wireless Communications*, 2025.
- [29] T. Zhao, S. Sarkar, E. Krijestorac, and D. Cabric, "Gan-rxa: A practical scalable solution to receiver-agnostic transmitter fingerprinting," *IEEE Transactions on Cognitive Communications and Networking*, vol. 10, no. 2, pp. 403–416, 2023.
- [30] Y. Zhang, Q. Li, H. Liu, L. Yang, and J. Yang, "Domain generalization for cross-receiver radio frequency fingerprint identification," *IEEE Internet of Things Journal*, 2024.
- [31] D. Kifer, S. Ben-David, and J. Gehrke, "Detecting change in data streams," in *VLDB*, vol. 4. Toronto, Canada, 2004, pp. 180–191.
- [32] I. Albuquerque, J. Monteiro, M. Darvishi, T. H. Falk, and I. Mitliagkas, "Generalizing to unseen domains via distribution matching," *arXiv preprint arXiv:1911.00804*, 2019.
- [33] H. Zhao, R. T. Des Combes, K. Zhang, and G. Gordon, "On learning invariant representations for domain adaptation," in *International conference on machine learning*. PMLR, 2019, pp. 7523–7532.
- [34] S. Ben-David, J. Blitzer, K. Crammer, A. Kulesza, F. Pereira, and J. W. Vaughan, "A theory of learning from different domains," *Machine learning*, vol. 79, pp. 151–175, 2010.
- [35] K. He, X. Zhang, S. Ren, and J. Sun, "Deep residual learning for image recognition," in *Proceedings of the IEEE conference on computer vision and pattern recognition*, 2016, pp. 770–778.
- [36] Y. Ganin, E. Ustinova, H. Ajakan, P. Germain, H. Larochelle, F. Laviolette, M. March, and V. Lempitsky, "Domain-adversarial training of neural networks," *Journal of machine learning research*, vol. 17, no. 59, pp. 1–35, 2016.